

A Two-fingered Underactuated Anthropomorphic Manipulator Based on Human Precision Manipulation Motions

Ian M. Bullock, *Student Member, IEEE* and Aaron M. Dollar, *Senior Member, IEEE*

Abstract— While designing robot hands based on grasping data is more common, fewer previous works have used details of human manipulation kinematics to improve robot hand design. The current work involves an underactuated, tendon driven, anthropomorphic manipulator with two flexor tendons and an abduction-adduction tendon, and describes its design based on experimental human precision manipulation data. Link lengths, joint axis alignment, and moment arms were derived from human subject data and values in the literature. The spring ratios, determining the torque relationships between joints, were then selected to maximize the achievable manipulation workspace from the human trial without requiring large forces, which are likely to lead to instability and object ejection. This is done by minimizing the stored spring energy in the robotic fingers across the range of precision manipulation workspace positions achieved by a representative human subject. After fabricating the hand, the energy characteristics of the resulting prototype are analyzed, and the robotic workspace is compared against the original human one. Despite only having three actuators, the hand is able to manipulate the test object within a 2.7 cm^3 workspace volume, compared to an average human workspace of 5.4 cm^3 for the same object. Future work could include adding antagonist actuators to achieve a larger motion range along the palmar-dorsal axis, which is currently the most limited axis of motion in comparison to the original human workspace.

I. INTRODUCTION

The human hand has impressive grasping and manipulation capability, and a great deal of effort has aimed at producing similar capability in robotic manipulators. Robot hand designs have been influenced by studies of human grasping kinematics, for example through the implementation of grasp synergies [1] in mechanical systems. However, fewer robotic hands have used detailed human manipulation data to inform design. The current work uses experimentally measured human precision manipulation kinematics to guide the design of an underactuated anthropomorphic manipulator (Fig. 1), by selecting kinematic and spring ratio parameters to allow the hand to execute similar within-hand manipulation motions to what human participants performed.

For this study, we focus on the thumb and index finger, which produce the largest precision within-hand manipulation workspace in humans [2] and are arguably the two most important digits for dexterous manipulation. While we keep an anthropomorphic kinematic structure, we focus on a much simpler actuation structure than the human hand (which incorporates about 15 muscle/tendon units for the thumb and

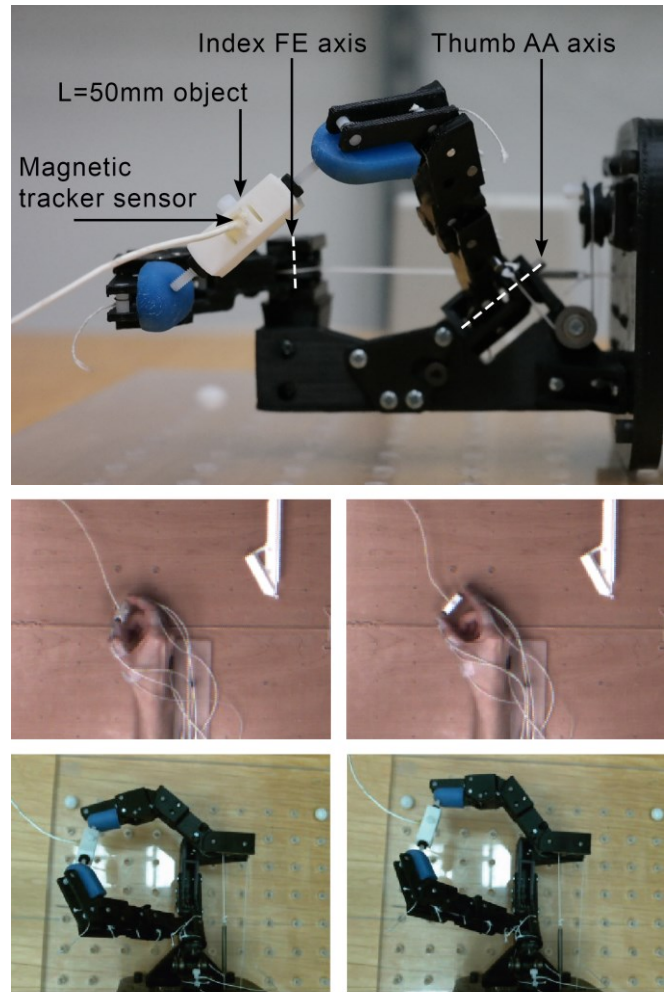


Figure 1. Robotic prototype, example human manipulation poses from the reference human workspace, and robotic pose examples (see also Fig. 6). Magnetic tracker sensors are used to capture the manipulation workspace, as well as the joint angles used by the human participant during manipulation.

index finger [3]) – one flexion actuator and tendon for each finger, and one ab/adductor for the thumb. This gives the possibility of manipulating an object in three degrees of freedom, while keeping mechanical complexity low. After designing and fabricating a prototype hand, the manipulation workspace is then experimentally measured and compared to the original human workspace.

Many anthropomorphic hands have been implemented with some precision within-hand manipulation capability, and a review can be found in [4]. A few works are particularly relevant to the current effort. Zollo et al. [5] selects robot

This work was supported in part by the National Science Foundation grants IIS-1317976 and IIS-0953856.

Ian M. Bullock and Aaron M. Dollar are with Yale University ({ian.bullock, aaron.dollar}@yale.edu), New Haven, CT, 06511.

finger spring constants based on simulations and to imitate a logarithmic spiral free swing fingertip trajectory. The present work differs by using human example motions to select the spring ratios. Some works such as the Anatomically Correct Testbed hand [6] have aimed to mimic the actuation and mechanical properties of the human hand very closely, but this typically involves a large actuator count and high mechanical complexity. The current work differs from this approach by using only a single flexor tendon on each finger, in addition to a single adduction-abduction actuator on the thumb.

One previous work uses a system identification approach to identify stiffness and damping properties of each index finger joint using small disturbances to a braced index finger [7]. These stiffness values are used in a robotic finger mechanism prototyping work [8], but that work focuses more on a novel mechanism for implementing non-linear spring behavior in a robotic finger. The spring constants identified through the system identification approach in [7], while a useful reference point, are not necessarily appropriate for direct usage in a robotic hand, since the robot hand may have a different actuation scheme from the human hand. The present work focuses on a novel spring ratio selection method based directly on human precision manipulation workspace data, and takes into account the specific kinematic parameters and simplified actuation scheme used.

The final product of the current work is the fabrication and experimental evaluation of a prototype two-fingered anthropomorphic manipulator. The performance is evaluated according to the range of Cartesian (x,y,z) positions over which a target object held in the fingertips can be manipulated in comparison with human subjects. While a large number of hands have been built that are anthropomorphic in structure [4] or otherwise designed to have dexterous within-hand manipulation capabilities (e.g. [9]–[11]), this is the first such quantitative comparison of robotic and human experimental manipulation workspace volume known in the literature. Benchmarking against human subjects is a sensible way to examine the “functional anthropomorphism” of a hand design.

The remaining sections of this paper proceed as follows. In section II, the methods for selecting the critical hand design parameters are described, including the selection of antagonist spring ratios based on the human manipulation workspace. In section III, the selected spring ratios, energy variation across the original human workspace, and a comparison of robotic and human workspace are presented. Finally, the results are analyzed in section IV, with a summary and future work in section V.

II. METHODS

Our general approach for this paper is to generate a prototype two-fingered hand that approaches the workspace capabilities of an average human subject manipulating a 50 mm object with the thumb and index finger (described in more detail in section III below) that also has low mechanical complexity. We use a single flexion tendon per finger, but add a third actuator for thumb adduction-abduction to facilitate out of plane manipulation and match the thumb’s available

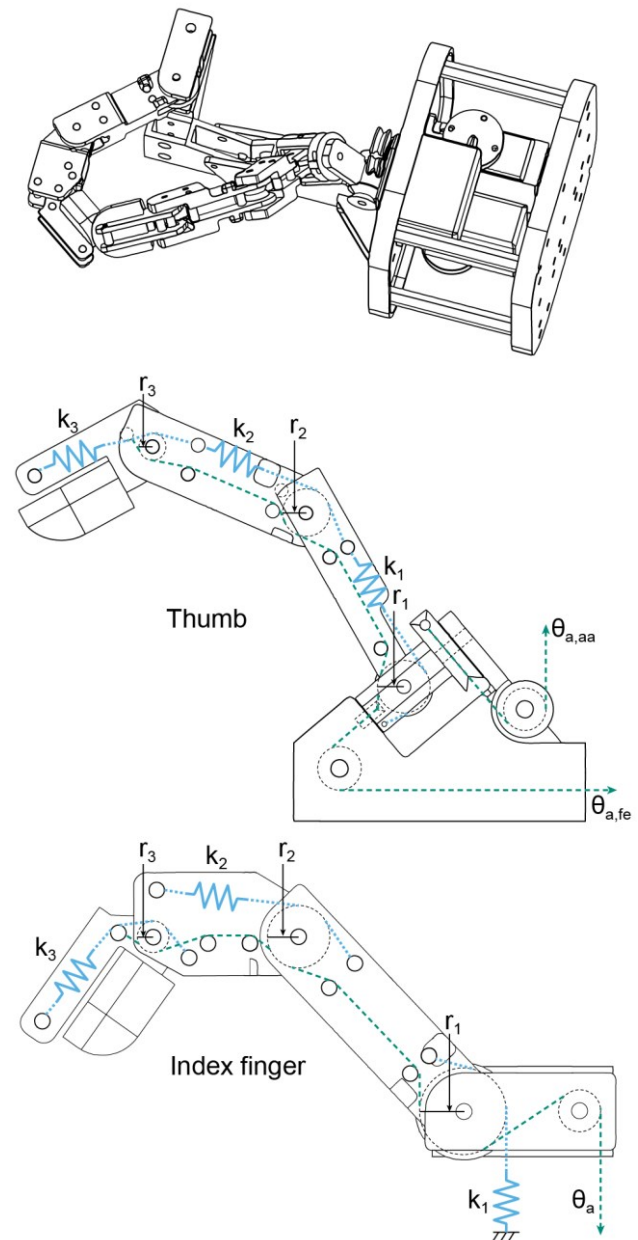


Figure 2. Prototype mechanical design. Routing is shown for the flexion actuator tendons in the thumb and index finger, as well as for the antagonist extension springs, which are routed to act in an equivalent manner to torsion springs. Thumb adduction-abduction actuation is also shown. Tangential connections to a pin or pulley indicate wrapping, while orthogonal connections indicate termination.

motions more closely to the human model. Many of the anthropomorphic hand design parameters such as link lengths and moment arms were adapted from the literature. Next, we applied a novel energy-based method to select appropriate antagonist spring ratios for the thumb and index fingers, based on detailed experimental human precision manipulation data. Finally, we used the spring ratios and other kinematic parameters to implement a prototype manipulator (Fig. 2), and compared its workspace to the original human workspace.

TABLE I. ANTHROPOMORPHIC JOINT MOMENT ARMS

Parameter	Moment arm (cm)	Scaled for prototype (cm)
Thumb CMC FE (Based on FPL)	1.45	0.59
Thumb MCP FE (Based on FPL)	0.99	0.40
Thumb IP FE (Based on FPL)	0.78	0.32
Index MCP FE (Based on FDP)	1.11	0.86
Index PIP FE (Based on FDP)	0.79	0.61
Index DIP FE (Based on FDP)	0.41	0.32

TABLE II. TARGET JOINT RANGE OF MOTION LIMITS

Parameter	Passive Range of Motion (°)	
	Flexion	Extension
Thumb CMC FE	17	28
Thumb MCP FE	54	10
Thumb IP FE	74	22
Index MCP FE	85	35
Index PIP FE	95	1
Index DIP FE	78	2

A. Anthropomorphic Kinematic Parameters

Joint positions and axis orientations were derived from a 50 pose MRI-based model [12] of a 29-year old female hand, implemented in OpenSim software [13]. The OpenSim kinematic parameters were ported to MATLAB and a few slight modifications performed to facilitate mechanical implementation. First, the entire model was rotated -12° around the x (palmar) axis in order to align the index finger flexion extension axis direction with the z-axis. The non-intersecting, non-orthogonal flexion-extension (FE) and abduction-adduction (AA) axes of the thumb carpometacarpal (CMC) joint were simplified as a single orthogonal, intersecting joint, centered at the average point between the original two axes. The final kinematic parameters derived from the MRI-based model for the robotic thumb and index finger are shown in Table I and II.

One flexor tendon is used for each finger, in addition to a directly driven abduction-adduction degree of freedom (DOF) in the thumb. Bio-inspired pulley ratios were selected based on moment arms for the tendons which terminate distally in the thumb and index finger, specifically the flexor pollicis longus (FPL) and flexor digitorum profundus (FDP). The thumb FPL moment arms were taken from [14] and the final values were produced by averaging the original values across the range of motion. The index FDP moment arms were taken from [15]. The moment arm ratios were kept consistent with these biologically inspired values, but were uniformly scaled down to facilitate mechanical implementation. Both the original human derived moment arms and the final scaled

TABLE III. JOINT CENTERS AND AXIS DIRECTIONS ADAPTED FROM STILLFRIED ET AL. MODEL.

Parameter	Location (cm) or vector orientation		
	x	y	z
Thumb CMC joint center	1.37	3.32	-0.68
Thumb CMC AA axis	0	-0.77	-0.64
Thumb CMC FE axis	1	0	0
Index MCP joint center	0.11	-2.88	0.35
Index MCP FE axis	0	0	1

TABLE IV. SEGMENT LENGTHS BASED ON DISTANCE BETWEEN CENTERS OF ROTATION IN STILLFRIED ET AL. MODEL

Parameter	Distance between centers of rotation (cm)
Thumb metacarpal length	4.53
Thumb proximal phalanx length	3.80
Thumb distal phalanx length	3.22
Index proximal phalanx length	4.74
Index intermediate phalanx length	2.86
Index distal phalanx length	2.22

values used in the mechanical prototype can be seen in Table III.

Finger passive motion limits in flexion and extension were taken from [16] and can be seen in Table IV. The joint extension limit angles were also used as zero force points for the extension springs in the prototype.

B. Spring Ratio Selection Based on Human Workspace

In the present work, we select spring ratios for the thumb and index finger by minimizing an undesirable energy increase from minimal energy finger configurations, across a previously measured human precision manipulation workspace. This method requires picking a representative human workspace, calculating energy values based on the finger joint angles across that workspace, and finally repeating this process for many different spring constants to identify an optimal spring ratio.

The comparison human data was taken from a study in which a range of human subjects manipulated various size objects within their fingertips to examine their maximum manipulation range [2]. For the hand design described in this paper, the reference human workspace trial was selected to be from a participant with close to average hand length (17.6 cm), as well as close to average workspace across the 16 participants studied. The manipulation trial involved a 50 mm length pointed object described in [17]. A representative workspace reference trial from this subject was selected to allow for the calculation of spring constants suited to typical manipulation motions.

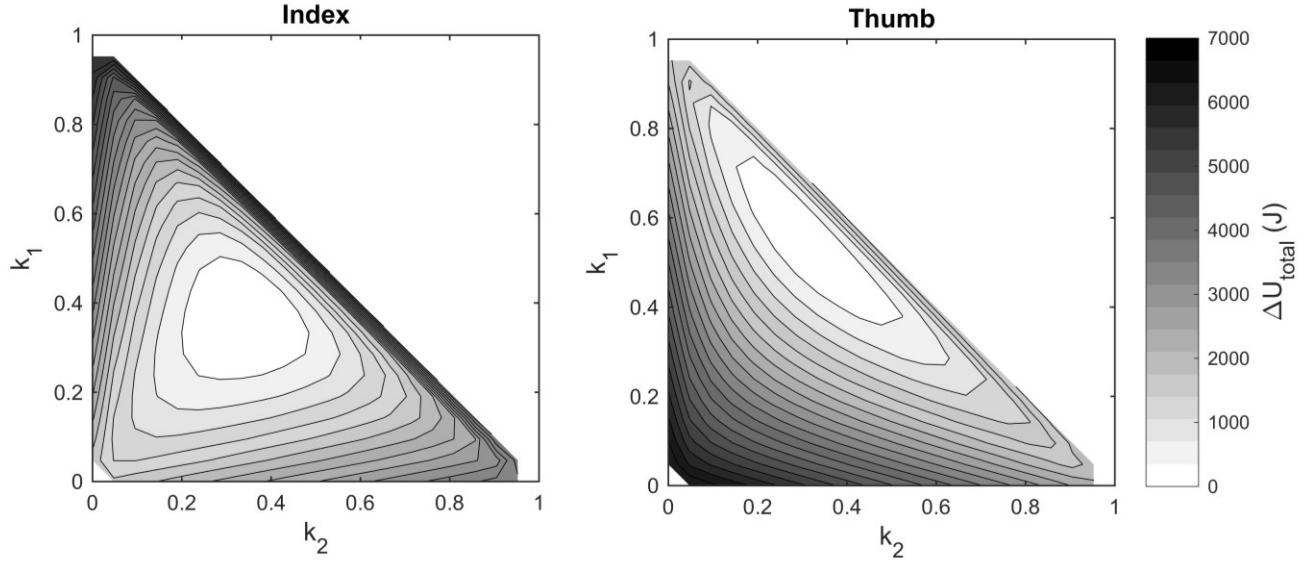


Figure 3. Energy difference (ΔU) contours for different spring ratios for the index finger and thumb. The spring constants are normalized in the initial optimization stage to add to 1. Thus, k_3 can be seen as a dependent variable of the other two spring constants. Smaller energy differences indicate better spring constants for mechanical implementation. The final index finger spring ratio is [0.42 0.32 0.26], while for the thumb it is [0.57 0.29 0.14].

Following selection of the reference human workspace, joint angles were calculated for each point in the workspace. The thumb and index finger are each modeled as 3-DOF planar fingers matched to the planar fingers of the robotic system. The finger modeling method is based on the formulations in [18], [19]. In the robotic prototype, each finger is driven under position control according to

$$\Delta \theta_a = J_a \Delta \theta = r_1 \Delta \theta_1 + r_2 \Delta \theta_2 + r_3 \Delta \theta_3, \quad (1)$$

where θ_a is the actuator angle, assuming a unit radius actuator pulley, and $\Delta \theta$ is the difference in the three angles from the extension limits, which are set to be the zero-force angles for the springs. Then, the stored energy in a finger can be computed as

$$U = \frac{1}{2} \Delta \vec{\theta} K \Delta \vec{\theta}^T = \frac{1}{2} (k_1 \Delta \theta_1^2 + k_2 \Delta \theta_2^2 + k_3 \Delta \theta_3^2). \quad (2)$$

For each point in the human workspace, this stored energy can be calculated based on the human joint angles and chosen spring constants. However, for a given point in the human workspace, it is also possible to calculate the finger energy if the object is removed, and the finger is allowed to reconfigure to its minimal energy configuration. This latter minimal configuration can be seen as the natural trajectory of the mechanism without external disturbances, and would be a point along the free-swing finger trajectory. First, we find the angles corresponding to the minimal energy configuration by taking partial derivatives $\frac{\partial U}{\partial \Delta \theta_1}$ and $\frac{\partial U}{\partial \Delta \theta_2}$, and equating them to zero. Solving the resulting equations yields:

$$\begin{aligned} \Delta \theta_{1,free} &= \frac{k_2 k_3 r_1}{k_2 k_3 r_1^2 + k_1 k_3 r_2^2 + k_1 k_2 r_3^2} \Delta \theta_a \\ \Delta \theta_{2,free} &= \frac{k_1 k_3 r_2}{k_2 k_3 r_1^2 + k_1 k_3 r_2^2 + k_1 k_2 r_3^2} \Delta \theta_a \\ \Delta \theta_{3,free} &= \frac{k_1 k_2 r_3}{k_2 k_3 r_1^2 + k_1 k_3 r_2^2 + k_1 k_2 r_3^2} \Delta \theta_a \end{aligned} \quad (3)$$

Given these three minimal-energy angles, which are calculated for the same tendon length (or $\Delta \theta_a$) as the original human angles, we can calculate a minimal energy value for that tendon configuration, by

$$U_{free} = \frac{1}{2} (k_1 \Delta \theta_{1,free}^2 + k_2 \Delta \theta_{2,free}^2 + k_3 \Delta \theta_{3,free}^2), \quad (4)$$

as in Equation 2.

Now, for each point in the human workspace, these energy values can be compared by computing:

$$\Delta U = U - U_{free}, \quad (5)$$

where ΔU is a function only of the recorded human $\Delta \vec{\theta}$ at that point and the chosen spring constants, since $\Delta \theta_a$ can be determined at each point using Equation 1 with the literature-derived tendon moment arms.

Finally, for a given set of candidate spring constants, we sum the individual ΔU values to compute an overall energy difference across the entire workspace, $\sum \Delta U_i = \Delta U_{total}$. We then use ΔU_{total} as our cost function to select an optimal spring ratio for the thumb and index finger individually. By reducing the overall extra energy stored in the system, the spring constants selected should produce a mechanism with natural behavior which is a good fit for typical manipulation motions, without unnecessary extra energy storage in the

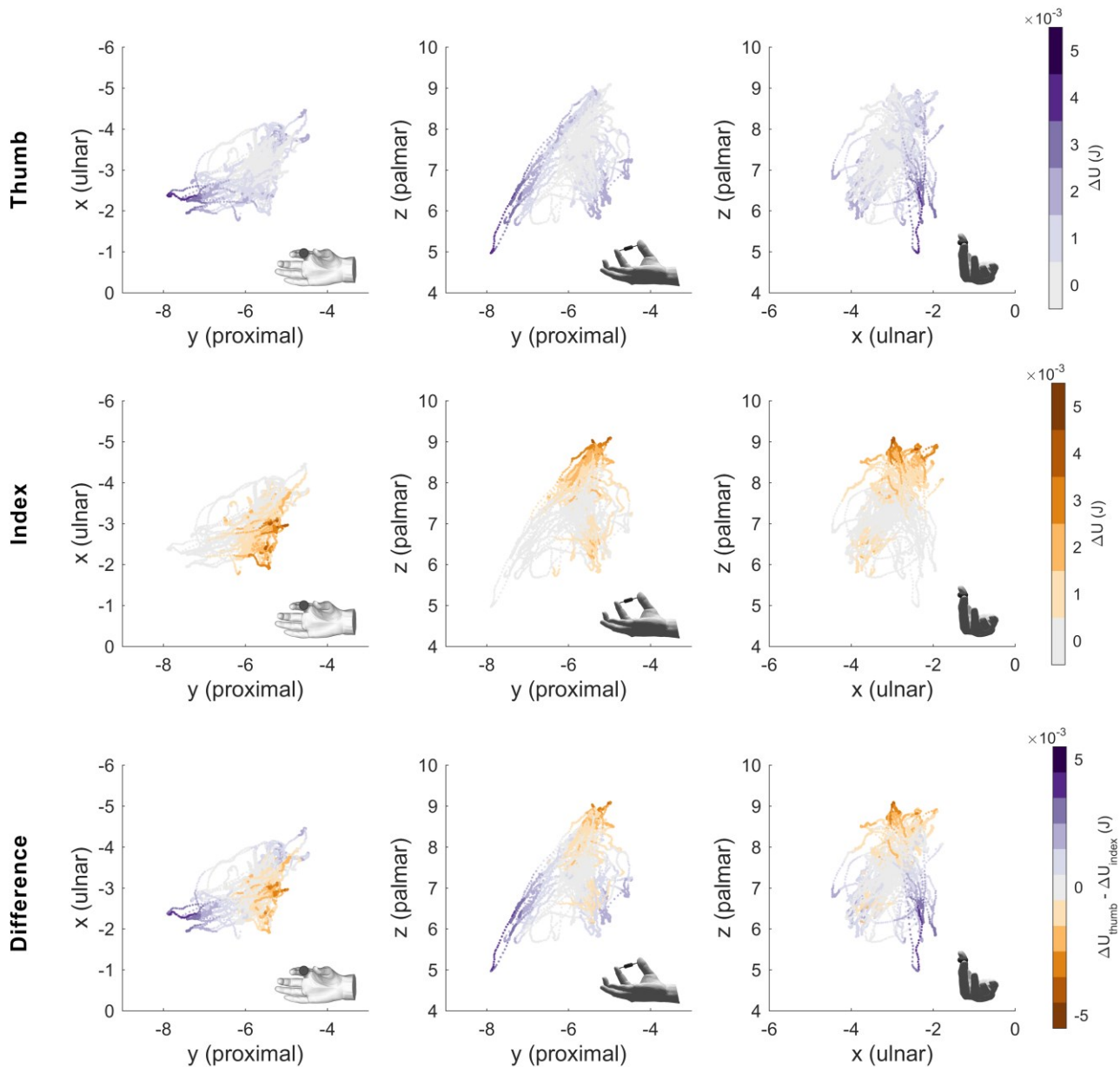


Figure 4. Energy difference (ΔU) for the selected spring constants across the original human workspace, plotted for the fingers individually, and also for the difference in stored energy between the two fingers. We observe a central region with lower ΔU , but certain regions have much higher ΔU values which may make stable robotic manipulation in those regions of the original human workspace difficult.

springs which would be likely to lead to manipulation instability.

One final step is to scale the spring constants from each individual finger to match them across the two fingers. In this case, we have uniformly scaled the final thumb spring constants slightly, while maintaining the same ratio, in order to have them match the overall ΔU_{total} between the thumb and index finger. Storing a similar amount of energy in each finger on average should be more appropriate than a manipulator where much more spring energy is stored in one digit than another.

C. Robotic Hand Test Implementation

Once the kinematic parameters and spring ratios have been selected, a robotic prototype can be constructed to compare its manipulation performance to that of the original human reference workspace. The hand was fabricated using ABS structural parts printed with an FDM printer at a 1:1 scale with the human hand it was modeled on. Holes in the ABS parts were then reamed to fit pins precisely. Steel pins were used to define joint rotation axes and support pulleys, while PTFE pins were used for the Spectra (45 kg test) tendon wrapping surfaces. V-groove bearings were used in a few locations as

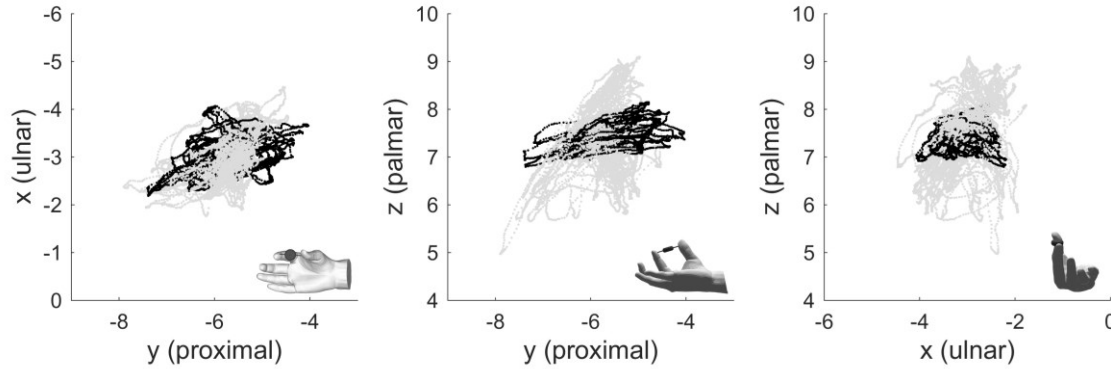


Figure 5. Comparison of experimental robotic (black) and human (gray) precision manipulation workspace. The robotic workspace is a combination of 12 separate short trials which all started and ended in the same location but used a wide variety of actuator motions. These 12 trials were selected as maximal workspace robotic trials out of 99 successful robotic trials which did not result in object ejection.

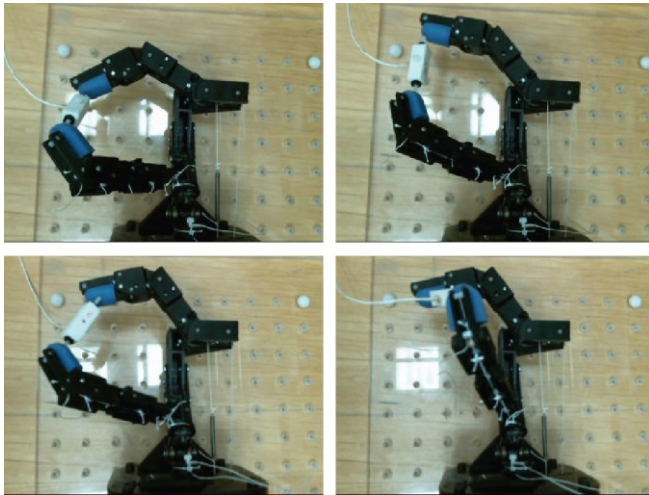


Figure 6. Four different example robotic hand poses taken from the high volume robotic trials.

low-friction pulleys for tendon routing. The blue fingertip shells were molded with shore 30A urethane rubber, and have a 2 mm outer shell thickness, with an internal plastic support and air pocket for additional compliance. Springs were made from longer extension spring stock by cutting to the calculated length and bending the ends. For actuation, three HD1501MG servos were used due to their favorable stall torque/price ratio and ease of control; they were position controlled through a Pololu Micro Maestro board via serial connection from MATLAB.

To evaluate robotic manipulation workspace, a series of 10 s manipulation trials were performed with randomized sinusoidal actuator trajectories, starting and ending from an initial position which was selected to closely match the average human finger-object angles discussed in [17]. The object was placed manually in the fingertips prior to each motion sequence for the current work. The sinusoidal trajectories given to each actuator were varied in both phase, amplitude, and frequency to give a wide variety of actuation combinations. Sinusoidal motions were used to avoid any sudden actuator movements which would likely lead to premature ejection of the object. The successful trajectories are then combined to provide a lower bound for the robotic

manipulation workspace, which can be compared to the reference human workspace.

III. RESULTS

Applying the energy based spring ratio optimization criteria discussed in II.B yields the energy contours shown in Fig. 3 for the thumb and index finger. Picking initial spring ratios for the thumb and index finger based on the minimum ΔU_{total} across the human workspace yields spring ratios, in order from proximal to distal, of $K_{thumb} = [0.57, 0.29, 0.14]$ and $K_{index} = [0.42, 0.32, 0.26]$. Following this initial optimization step, K_{thumb} was scaled uniformly to ensure that

$$\Delta U_{total}(K_{thumb}, \Theta_{thumb}) = \Delta U_{total}(K_{index}, \Theta_{index}), \quad (6)$$

where the total energy difference is a function of the spring constants as well as the full set of joint angles across the reference human workspace. This results in a final $K_{thumb} = [0.76, 0.38, 0.19]$. Finally, it is necessary to uniformly scale the six unitless values from both fingers to real-world physical spring constants. The final scaling involves spring constants in a similar overall range to related works such as [5], but was chosen in part due to packaging constraints and readily available commercial springs. Specifically, the final target spring constants implemented are $K_{thumb} = [0.016, 0.0078, 0.0039] N \cdot m/rad$ and $K_{index} = [0.0086, 0.0065, 0.0054] N \cdot m/rad$. These torsional spring constants were converted to linear spring constants using the joint moment arms and implemented with cut-to-length extension springs, in order to match the target spring constants as closely as possible. The material for each spring was selected from multiple possible wire thicknesses in order to achieve the desired spring constant within the length ranges imposed by prototype space constraints.

After selecting spring ratios, it is possible to evaluate the pattern of energy variation across the original space of human workspace points, as shown in Fig. 4. Specifically, for each point in the original workspace and for the chosen spring constants, the excess energy ΔU is calculated at each point relative to the minimum energy configuration of the finger for the tendon length required to achieve the corresponding finger

joint angles. The only difference from the spring constant selection phase is that the ΔU is plotted at individual points, rather than being summed across the entire workspace. Overall, the thumb and index finger plots show a central region with fairly small ΔU . We expect particularly large ΔU values to correlate with regions where it is difficult for the final robotic prototype to stably manipulate the object. The final row shows the difference in ΔU between the thumb and index fingers across the human workspace.

After finding the target spring stiffnesses, the desired springs were implemented in to the mechanical hardware (described in section III.C. above). The workspace of the hand manipulating the 50mm object was then experimentally evaluated, and compared to the human workspace (Fig. 5). Overall, 99 successful 10-second robotic manipulation motions were performed using a wide variety of actuator inputs. From this set of 99 trials, 12 maximal workspace trials were selected and combined into the single robotic trial shown in Fig. 5. The final robotic workspace for this 12-trial composite is 2.71 cm³, compared to 2.97 cm³ for the combination of all 99 robotic trials. Since there is not a large difference in the 12 and 99 trial volumes, the selected 12 trials should capture most of the robotic range of motion. Combining 12 trials produces the same number of sample points (9600 points across 120 s) as the human trial, which achieved 5.4 cm³ workspace. Fig. 6 shows example manipulation poses for the robotic hand from the high workspace volume trials.

IV. DISCUSSION

Overall, the simplified, three-actuator anthropomorphic manipulator was able to achieve 50% of the human workspace through imitation of many of the human kinematic parameters and careful selection of antagonist springs. In comparison to stiffness values from the literature, the selected index finger spring ratio of [0.42 0.32 0.26] can be compared the system identification based values in [7], namely [0.34 0.54 0.11]. In the work of Zollo et al. [5], initial optimization gave spring ratios of [0.48 0.30 0.22] with $r = [7\ 3\ 2]$ mm, which are similar to the present work, but optimizing for a logarithmic spiral free-swing trajectory then gave [0.31 0.35 0.34]. That latter approach of optimizing around a spiral free-swing trajectory might be better suited for power grasping functionality of the hand and it is not surprising that it yields different values from the current work. The ratio of Kamper et al. [7] with very low DIP joint stiffness may not be well suited to the current actuator scheme with a single flexor tendon, since this would likely lead to a much greater degree of DIP joint flexion which would make stable precision manipulation difficult.

In general, the chosen spring constants produce a central region of small ΔU , as shown in Fig. 4, which helps to confirm that the selected spring constants are appropriate. However, particularly high energy offsets are observed in the extremes of the palmar axis direction, for example. The robotic workspace, while including 50 % of the human workspace overall, does not extend into these high energy regions in the furthest palmar and dorsal ranges.

In the proximal-ulnar plane, however, some of the high ΔU regions appear to still allow stable robotic manipulation. In this case, we see a fairly gradual shift from the thumb being at a higher energy state toward the distal direction, and the index finger being at a higher energy state in the proximal direction. It is possible that the energy differences along the proximal-distal axis are smoother and thus less likely to lead to object ejection than the changes along the palmar-dorsal axis.

V. CONCLUSION AND FUTURE WORK

Overall, this work presents the design of a two-fingered anthropomorphic hand based on a range of human subject data, as well as a novel energy-based approach for selecting spring ratios based directly on experimentally measured human precision manipulation motions. The prototype three-actuator manipulator is able to achieve greater than 50% of the average human workspace, despite only utilizing three actuators (in comparison with the roughly 15 muscle/tendon units in the human thumb and index finger). It can be reasonably expected that this performance might be extended even further by increasing the number of actuators in the system or implementing a more sophisticated feedback control scheme. While the current work focuses on position of the object, control of object orientation could be important for some manipulation tasks.

In future work we would like to expand on the initial two-fingered hand prototype presented here to create a complete and fully-integrated anthropomorphic dexterous hand design. Among other tasks, this will involve addressing the design of the other three fingers of the hand, as well as developing a more robust and refined hand structure that implements a fully anthropomorphic shape with all of the actuators embedded within the structure. Direct extensions of the work presented in this paper include modifying the hand design to reach additional parts of the workspace which are currently difficult to reach, such as by adding additional actuators, especially antagonists.

ACKNOWLEDGMENT

The authors acknowledge Joseph Belter, Thomas Feix, and Raymond Ma for helpful discussions related to the methods used in this work.

REFERENCES

- [1] M. Santello, M. Flanders, and J. F. Soechting, "Postural Hand Synergies for Tool Use," *J. Neurosci.*, vol. 18, no. 23, pp. 10105–10115, Dec. 1998.
- [2] I. M. Bullock, T. Feix, and A. M. Dollar, "Human Precision Manipulation Workspace: Effects of Object Size and Number of Fingers Used," in *Engineering in Medicine and Biology Conference*, 2015.
- [3] I. A. Kapandji, *The Physiology of the Joints*, 2nd ed. New York: Churchill Livingstone, 1982.
- [4] L. Biagiotti, F. Lotti, C. Melchiorri, and G. Vassura, "How Far is the Human Hand? A Review on Anthropomorphic End Effectors," 2004.
- [5] L. Zollo, S. Roccella, E. Guglielmelli, M. C. Carrozza, and P. Dario, "Biomechatronic design and control of an anthropomorphic artificial

- hand for prosthetic and robotic applications,” *IEEE/ASME Trans. Mechatronics*, vol. 12, no. 4, pp. 418–429, 2007.
- [6] N. Gialias and Y. Matsuoka, “Muscle actuator design for the ACT Hand,” in *IEEE International Conference on Robotics and Automation*, 2004, pp. 3380–3385.
- [7] D. G. Kamper, T. George Hornby, and W. Z. Rymer, “Extrinsic flexor muscles generate concurrent flexion of all three finger joints,” *J. Biomech.*, vol. 35, no. 12, pp. 1581–1589, 2002.
- [8] P.-H. Kuo, J. Debacker, and A. D. Deshpande, “Design of Robotic Fingers with Human-like Passive Parallel Compliance,” in *IEEE International Conference on Robotics and Automation*, 2015, pp. 2562–2567.
- [9] K. Tahara, K. Maruta, and M. Yamamoto, “External sensorless dynamic object manipulation by a dual soft-fingered robotic hand with torsional fingertip motion,” in *IEEE International Conference on Robotics and Automation*, 2010, pp. 4309–4314.
- [10] L. U. Odhner and A. M. Dollar, “Dexterous manipulation with underactuated elastic hands,” in *IEEE International Conference on Robotics and Automation*, 2011, pp. 5254–5260.
- [11] M. T. Mason, a. Rodriguez, S. S. Srinivasa, and a. S. Vazquez, “Autonomous manipulation with a general-purpose simple hand,” *Int. J. Rob. Res.*, vol. 31, no. 5, pp. 688–703, Dec. 2011.
- [12] G. Stillfried, U. Hillenbrand, M. Settles, and P. Van Der Smagt, “MRI-based skeletal hand movement model,” in *The Human Hand: A Source of Inspiration for Robotic Hands. Springer Tracts on Advanced Robotics*, Switzerland: Springer International Publishing, 2014, pp. 49–76.
- [13] S. L. Delp, F. C. Anderson, A. S. Arnold, P. Loan, A. Habib, C. T. John, E. Guendelman, and D. G. Thelen, “OpenSim: open-source software to create and analyze dynamic simulations of movement,” *IEEE Trans. Biomed. Eng.*, vol. 54, no. 11, pp. 1940–50, Nov. 2007.
- [14] W. Paul Smutz, A. Kongsayreepong, R. E. Hughes, G. Niebur, W. P. Cooney, and K. N. An, “Mechanical advantage of the thumb muscles,” *J. Biomech.*, vol. 31, no. 6, pp. 565–570, 1998.
- [15] K. N. An, Y. Ueba, E. Y. Chao, W. P. Cooney, and R. L. Linscheid, “Tendon excursion and moment arm of index finger muscles,” *J. Biomech.*, vol. 16, no. 6, pp. 419–425, 1983.
- [16] N. a. Davidoff and A. Freivalds, “A graphic model of the human hand using CATIA,” *Int. J. Ind. Ergon.*, vol. 12, no. 4, pp. 255–264, 1993.
- [17] I. Bullock, T. Feix, and A. Dollar, “Workspace Shape and Characteristics for Human Two- and Three-Fingered Precision Manipulation,” *IEEE Trans. Biomed. Eng.*, vol. 62, no. 9, pp. 2196–2207, 2015.
- [18] R. R. Ma and A. M. Dollar, “Linkage-based Analysis and Optimization of an Underactuated Planar Manipulator for In-Hand Manipulation,” *J. Mech. Robot.*, pp. 1–11, in press.
- [19] R. Balasubramanian, J. T. Belter, and A. M. Dollar, “Disturbance Response of Two-Link Underactuated Serial-Link Chains,” *J. Mech. Robot.*, vol. 4, no. 2, p. 021013, 2012.